Long-term wave load trends against offshore monopile structures: A case study in the Bay of Biscay

Nahia Martinez-Iturricastillo, Alain Ulazia, and John V. Ringwood

Abstract—**This study examines the trend in wave parameters over available annual records in the Bay of Biscay. The aim is to study the effect of the significant wave height (H_s), peak wave period (T_p), and corresponding loads on monopile cylindrical structures, which are basic component structures for wave energy converters and offshore wind turbines. The work presented is a first approach to understand the wave trend over the analysed time period (1900-2010), with the hope that a better characterization of the wave resource could help to provide important design information for future wave energy technology. The effect of this evolution, against monopile structures is studied using the 20th century reanalysis ERA20 (1900-2010) from ECMWF (European Centre for Medium-Range Weather Forecasts), calibrated versus reanalysis ERA5. Based on the benchmark 5MW NREL fixed monopile turbine, a significant increase in wave drag forces, inertial forces, and fore-aft moment, of up to 15%, is computed over 111 years at a gridpoint near the Western Basque coast, constituting a strong positive slope that can be clearly associated with climate change, and has strong implications for the design of new marine renewable energy technology.**

Index Terms—**Monopile wave loads, ERA20, ERA5, wave trend, Bay of Biscay**

List of Abbreviations

ECMWF	European Center for Medium-Range Weather Forecasts
BiMEP	Biscay Marine Energy Platform
POEM	Plan de Ordenación del Espacio Marítimo
OWC	Oscillating Water Column
GP	Grid Point
NOA	North Atlantic Oscillation
CI	Confidence Interval

This publication is part of a Grant from Science Foundation Ireland under Grant number 18/CRT/6049. This paper is also part of project PID2020-116153RB-I00 funded by MCIN/AEI/10.13039/501100011033 and has also received funding from the University of the Basque Country (UPV/EHU project GIU20/08).

Nahia Martinez-Iturricastillo working in the Centre for Ocean Energy Research (COER), Maynooth University, Maynooth, Co. Kildare, Ireland (e-mail: nahia.martineziturricastillo.2023@mumail.ie).

Alain Ulazia is with the Energy Engineering Department, University of the Basque Country (UPV/EHU). Engineering School of Gipuzkoa-Eibar (e-mail: alain.ulazia@ehu.eus).

John V. Ringwood director of the Centre for Ocean Energy Research (COER), Maynooth University, Maynooth, Co. Kildare, Ireland (e-mail: john.ringwood@mu.ie).

Digital Object Identifier:
https://doi.org/10.36688/ewtec-2023-paper-275

Nomenclature

C_D	Drag coefficient
C_I	Inertial coefficient
D	Tower diameter
d	Water depth
F_D	Drag force
F_I	Inertial force
g	Gravity constant (9.8 m/s^2)
H_s	Significant wave height
k	Wave number
L	Monopile length (m)
M_I, M_D	Inertial and drag moment (kNm)
T_p	Peak wave period
ρ_w	Density of sea water ($\approx 1030 kg/m^3$)
ρ_a	Air density (kg/m^3)
ζ	Wave amplitude for regular waves

I. Introduction

BASQUE people have always had a strong connection to the sea, fishing played an important role in the economy while also serving as a significant source of food. During the XVIth century, whale hunting was particularly notable as a fishing practice [1]. During the first industrial revolution, the connection between Bilbao and United Kingdom was made through the sea enabling the transport of iron [2]. Nowadays several activities take place in the Bay of Biscay such as surf, fisheries, or cargo and people transport. In the early future, and together with the development of marine renewable technologies, this space will also be shared with this new coming solution.

There is a clear interest in the Basque Country for marine renewable technologies to develop. There are different research groups working in this area [3], universities offering training [4] and companies developing technologies. Moreover, in the past year, there have been various conferences and events supporting the development of these technologies [5]–[7]. At the Biscay Marine Energy Platform (BiMEP) it is possible to test various devices and technologies, such as, wave energy devices, prototypes of floating offshore wind, offshore wind turbines, but also fixed foundations for offshore wind [8], which is the topic being analysed in this paper.

Earlier in 2023, the Spanish Goverment published the POEM (Plan de Ordenación del Espacio Marítimo), which aims to regulate and promote sustainable activities in the marine environment, considering various ecological, economic, and social factors, so the marine environment is preserved. Wave and wind resource in the Bay of Biscay are also analysed, the average wave

potential at the nearest Basque coast is $20kW/m$, while the wind energy potential range is $400 - 500W/m^2$ [9].

In the future, by 2100, it is predicted that the significant wave height will decrease, but extreme events will be more frequent [10]. With this in mind, this first approach aims to analyse the trend of the significant wave height (H_s) and peak wave period (T_p) in the Bay of Biscay from 1900 until 2010, and calculate the loads of these waves against a fixed monopile structure of six meter diameter at twenty meter depth, which are the characteristics of the NREL OC3 monopile described and used in varios works such as [11] (Figure 1).

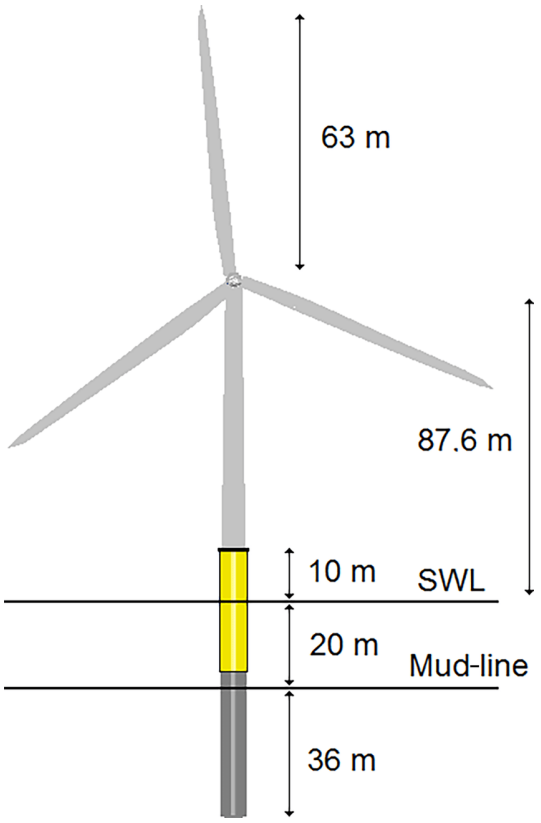

Fig. 1. NREL OC3 monopile supporting a 5 MW benhmark wind turbine [11]. The total length of the monopile is 30 m but there is 20 m below sea level (SWL). It is embedded in the seabed to the depth of 36 meters.

II. Data and Methodology

A. Data

In order to analyse the wave loads trend, two different datasets from ECMWF (European Centre for Medium-Range Weather Forecasts) are used, ERA20 and ERA5. The features of the reanalysis from both these datasets are summarized in Table II-A2.

1) ERA5 reanalysis: ERA5 is a reanalysis dataset of the global climate that provides hourly estimates of atmospheric, land, and oceanic climate variables. It is the fifth generation of atmospheric reanalysis produced by the ECMWF after ERA-40, ERA-Interim or ERA20C, and covers the period from January 1940 to present in the Copernicus Data Store [12]. ERA5 reanalysis is available at single levels pressure levels, with a preliminary dataset from 1950 to 1978 also available on the Copernicus Climate Data Store. The data cover the Earth surface on a 30km grid and resolve the atmosphere using 137 levels from the surface up to a height of 80km. ERA5 includes uncertainty information for all variables at reduced spatial and temporal resolutions [13].

TABLE I
Features of ERA20 and ERA5

Reanalysis	Period covered	Space resolution	Time resolution
ERA20	1900-2010	125 km	3 h
ERA5	1970-Present	30 km	1 h

2) ERA20 reanalysis: ERA-20C (ERA20 here), in contrast, is ECMWF's first atmospheric reanalysis of the 20th century, spanning from 1900-2010. It is a comprehensive, gridded dataset of many climate variables that assimilates observations of surface pressure and surface marine winds only from satelites after 1970, and ICOADs marine dataset of nautical in-situ measurements after 1900 [14]. ERA-20C is an outcome of the ERA-CLIM project, which aims to produce high-quality reanalysis datasets for the 20th century, using advanced data assimilation systems and state-of-the-art climate models. The reanalysis provides global atmospheric and surface data on a daily, invariant, and monthly mean basis, which can be sliced along any dimension of interest, serving many applications. The observation feedback archive of ERA-20C includes observation departures, not only for assimilated observables but also for non-assimilated ones, such as temperature and humidity measured by ships, buoys, and platforms at sea or on sea-ice [15].

It should be noted that the 125 km spatial resolution of this reanalysis is a necessary spatial information loss to gain a long time interval of more than a century, which is sufficient to neutralize the contribution of climatic teleconnection patterns such as El Niño/a, NOA (North Atlantic Oscillation), etc [16]. It is therefore hypothesized that a grid cell, corresponding to a selected grid point, comprises an area of 125x125 km, where the input historical time series of wave height and period can be considered suitable.

3) Selected parameters and study area: The analysed parameters are significant wave height H_s and peak wave period T_p. Monthly data from 1900 until 2010 are analysed in the area represented in Figure 2, a total of 14 grid points (GP). The results presented in this paper belong to the grid point indicated in red in Figure 2 (Longitude: $-3°$ W, Latitude: $44.5°N$). As stated before, with a spatial resolution of ERA20 of 125 km, it is hypothesised that the GP represents an area of 125x125 km. This grid point is the nearest point to the Basque Country and therefore the nearest point to Bilbao, whee EWTEC is being held, or to Armintza, where BiMEP is located.

4) NREL OC3 monopile: Wave loads against a monopile structure are calculated. The selected monopile is the OC3 monopile from NREL5 [17]. The features of the OC3 monopile are listed in Table II-A4. As shown in Figure 1, the monopile extends from the seabed up to ten meters above the mean water level, so

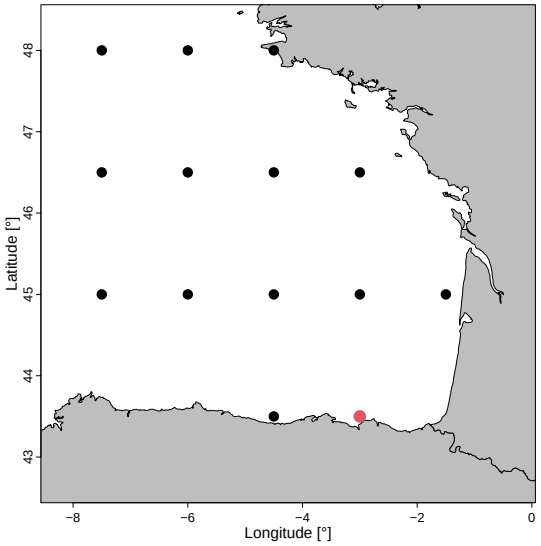

Fig. 2. Analysed area in this case study, in red colour the studied gridpoint near BiMEP, in the East of Basque coast (Longitude: $-3°$ W, Latitude: $44.5° N$).

TABLE II
CHARACTERISTICS OF THE OC3 MONOPILE.

Item	Value	Unit
Monopile length	30	m
Transition piece height	10	m
Monopile embedded depth	30	m
Monopile diameter	6	m
Monopile thickness	60	mm

the submerged part of the monopile extrends to twenty meters [17].

5) Trend computation: Although ERA20 vs ERA5 bias correction is developed using 3h data, monthly data of the calibrated series are represented for the visualization of the trend. The slope line is computed using the Theil-Sen method [18], which computes a more robust trend using medians instead of average values, avoiding deviations due to outliers.

Furthermore, a dashed area is computed around the slopes according to the CI (Confidence Interval) at 95%, which establishes a way to certify the significance of these trends (see the figures of the Section III).

B. Methodology

1) Quantile matching: As shown in Figure 3, data was calibrated via a quantile matching technique, ERA20 was calibrated against the ERA5 nearest grid point, within the 1970-2010 time frame, obtaining as a result the calibrated ERA20C. This technique has been previously used in climatology-related literature for calibration of temperature, wind speed, or precipitation [19]–[24]. The main characteristic of this kind of calibration is based on the correction of the bias with respect to the observation, this calibration technique was also used for studies of historical trends on wave

TABLE III
RESULTS FOR THE DIMENSIONLESS AXIS OF LE MÉHAUTÉ'S GRAPH.

T_p [s]	H_s [m]	X axis	Y axis
7.10	0.52	0.0405	0.00105
10.40	0.93	0.0189	0.00087
14.70	1.90	0.0094	0.00089

energy in the Bay of Biscay [25], Chile [26], and Ireland [27]. There is the possibility of categorization of this calibration technique via spatial, directional, or temporal criteria (spatial distribution, mean wave direction, or seasonality) to obtain a more robust bias correction [28], [29], which could be used in future studies due to the importance of directionallity in shallow water.

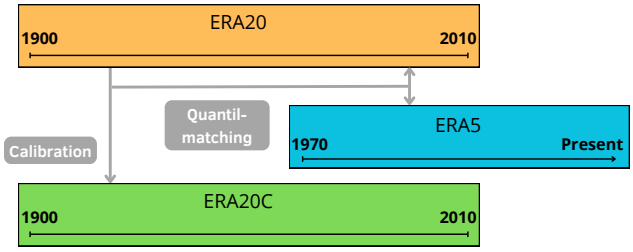

Fig. 3. Flow diagram of calibration (bias correction) of data via quantile-matching using ERA20 vs ERA5 reanalysis. ERA20 was calibrated against the closest ERA5 grid point, within the 1970-2010 time frame, obtaining as a result the calibrated ERA20C for the entire period 1900-2010.

2) Le Méhauté wave diagram: To select the model used to analyse the wave loads, a preliminary analysis of the data was made by analysing Le Méhauté's wave diagram. The diagram is composed of two dimensionless axis, expressed in Equation (1) and (2), H being the significant wave height, T the wave period, and d the ocean depth of the analysed grid point coordinates [30].

$$LeMéhauté_x = \frac{d}{gT^2} \tag{1}$$

$$LeMéhauté_y = \frac{H}{gT^2} \tag{2}$$

The limits of the area enclosed in Figure 4 are represented in Table II-B2. The limits of both dimensionless variables have been calculated by applying Equation (1) and (2). Where T and H are obtained from ERA5 (1981-2010) at a 95% confidence interval for the analysed grid point. The wave dispersion law relation is applied to articulate the transition from deep water to shallow water with the corresponding reduction of wavelength and wave height, according to linear approximation [31].

The area enclosed in Figure 4 encompasses two wave theories, Stokes' second order and linear or Airy model theory. Previous studies demonstrated that applying Stokes' second-order theory does not differ much from the Airy model, with regards to the overall dynamics and support of the monopile [32]. Consequently, for this particular project, Airy wave theory was employed as a good approximation.

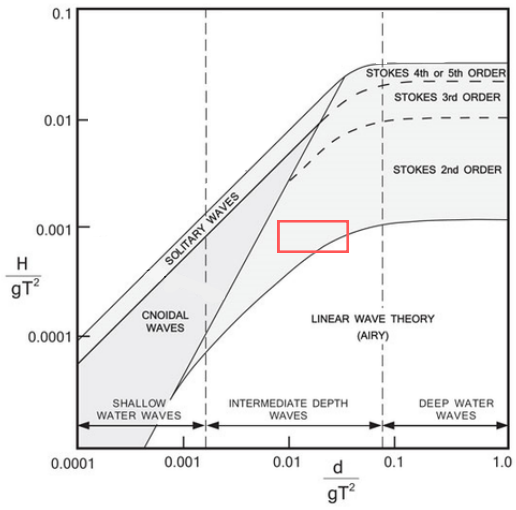

Fig. 4. Le Méhauté wave diagram where the red square represents the analysed wave range according to 1h ERA5 data in the nearest gridpoint selected at 95% CI for H_s and T_p (period 1980-2010).

3) Airy wave theory: In the Airy model the amplitude ζ is half the wave height: $\zeta = H/2$. The wave number $k = 2\pi/L$, is inversely proportional to the wavelength. The wavelength which can be computed using the Airy model of regular waves as a function of the wave period by applying the dispersion law, expression in Equation 3.

Equations (4) and (5) show, respectively, expressions for the inertial force F_I and drag force F_D induced by waves against a cylindrical tower of diameter D at a water depth d, with gravity constant $g = 9.8m/s^2$ and sea water density $\rho_w \approx 1025kg/m^3$. The drag constant C_D is 1.5 for cylindrical structures, and C_m is the inertial constant with a value of 2 for smooth cylinder [33]. This inertial effect described by the Morison equation [34] contains the sum of the Froude-Kyrlov force and the hydrodynamic mass force, and is related to the acceleration of water particles within the wave circulation [35].

$$L = \frac{gT^2}{2\pi}\tanh(kd) \tag{3}$$

$$F_I = \rho_w g \frac{C_m \pi D^2}{4}\hat{\zeta}\tanh(kd) \tag{4}$$

$$F_D = \rho_w g \frac{C_d D}{2}\hat{\zeta}^2\left[\frac{1}{2} + \frac{kd}{\sinh(2kd)}\right] \tag{5}$$

$$M_I = \rho_w g \frac{C_m \pi D^2}{4}\hat{\zeta}d\left[\tanh(kd) + \frac{1}{kd}\left(\frac{1}{\cosh(kd)} - 1\right)\right] \tag{6}$$

$$M_D = \rho_w g \frac{C_d D}{2}\hat{\zeta}^2\left[\frac{d}{2} + \frac{2(kd)^2 + 1 - \cosh(2kd)}{4k\sinh(2kd)}\right] \tag{7}$$

The total moment on the seabed M_{tot} is calculated from the sum of inertial and drag moments as in Equations (6), (7) and (8).

$$M_{tot} = M_I + M_D \tag{8}$$

4) OpenFAST simulation: NREL OpenFAST is an open-source wind turbine simulation tool that enables the analysis of a range of wind turbine configurations, including two- or three-blade horizontal-axis rotors, pitch or stall regulation, and more. It is the framework (or "glue code") that couples computational modules for aerodynamics, hydrodynamics for offshore structures, control and electrical system (servo) dynamics, and structural dynamics to enable coupled nonlinear aero-hydro-servo-elastic simulation in the time domain [36]. It represents a transition to better support an open-source developer community across research laboratories, industry, and academia around FAST-based aero-hydro-servo-elastic engineering models of wind-turbines and wind-plants, including files $Aerodyn$ for aerodynamics and $Hydrodyn$ for wave simulations in offshore wind turbines such as the selected fixed monopile at 20 m depth, together with floating systems, or jacket fixed structures [32].

III. Results

Validation of the model using OpenFAST for wind turbine monopile

In order to validate the proposed methodology, the results obtained applying Equation (8) are compared to a FAST simulation in which the effect of air is disregarded in the $Aerodyn$ input file ($\rho_a = 0$). As a result, the loads against the monopile are solely generated by waves. The introduction of second-order waves, or irregular waves via the Perason-Moskovich distribution [37], does not substantially affect the results.

A simulation has been carried out for a wave amplitude of 2 meters and wave period of 10 meters at a depth of 20 meters, according to Figure 5a. The fore-aft moment generated by such a wave in the FAST simulation is compared to the Airy model total moment, calculated as the sum of the drag and inertial moments. For these conditions, the maximum moment in the FAST simulation is 4867 kNm, while the lowest values is -7914 kNm, occurring in a 50 seconds frame, generating five waves. With the aim of analysing the long-term loads trends, for that same scenario ($H_s = 2m$, $T_p = 10s$, $d = 20m$), the total moment the waves generate against the monopile at the seabed is $M_{tot} = 4,400kNm$, represented in red in Figure 5b [17].

Although the Airy model captures the positive fore-aft moment almost perfectly, and the results are not affected by second-order effects (see the diagram of Figure 4) or irregular waves, the negative moment and the standard deviation of our deterministic method should be improved in future research.

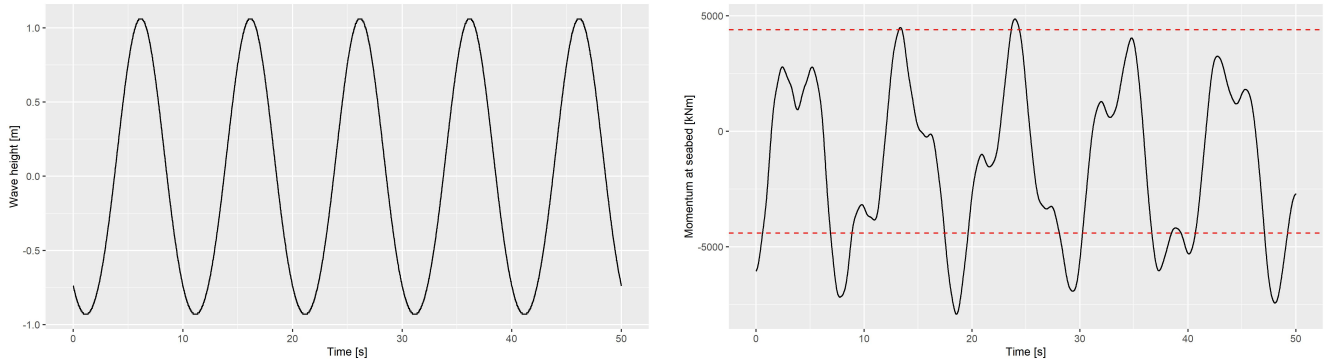

(a) FAST simulation H_s (b) Fast simulation M_{tot}

Fig. 5. Model validation, comparison of results and OpenFAST simulation for regular, irregular and second-order waves against the referential monopile. The fore-aft torque obtained with the deterministic long-term model offers a good preliminary validation against OpenFAST simulations.

Wave trends and the corresponding load trends

As explained in SectionII-A3, the results presented in Figures 6, 7, and 8 correspond to the nearest grid point to the Basque Country, the GP in red in Figure 2. Monthly data from 1900 to 2010 is represented in dots while the trend is in red.

In Figure 6, the evolution of significant wave height and peak wave period is represented for the analysed location. There is an increasing trend for both variables: significant increment at 95% confidence level between 15% and 20% per century. Average calibrated monthly H_s goes from 0.8 m to above 1.1 m, and T_p goes from 9.5 s to 10.5 sec.

For calculating the loads, inertial and drag force, shown in Figure 7, Equation (5) and (4) have been applied to each monthly combination of H_s and T_p. There is a clear increase in both forces around 15% in inertial force and around 40% increase in drag force.

Lastly, the total momentum has been calculated. The momentum the monopile would stand at seabed level is calculated by summing up both drag and inertial momentum; the expressions to measure those are in Equation (6) and (7), giving the resultant total value in Equation (8).

IV. Conclusions

While previous work [10] forecasts a future decrease in significant wave height for 2100 in different scenarios of climate change, the past time frame analysed in this paper(1900-2010), representing the transition from pre-industrial era to industrial era, shows an increasing trend over the last century that can reach the 15-20%. This is also reflected in the loads offshore monopile structures must withstand, which also increase over the years in a similar proportion to drag and inertial forces, supported by the benchmark OC3 NREL monopile, and their related fore-aft moment with respect to the seabed. An obvious first conclusion of this significant increment is the need to impose a higher steel thickness in the monopile to limit the fore-aft displacement at its extremum.

Future research should improve the uncertainties presented in this linear model, although second order effects have been shown to be insignificant for wave loads and moments in the verification of different wave-structure interaction models including $OpenFAST$ for our referential monopile [32]. Furthermore, the influence of non-linealities can be included by statistical treatment of the likelihood of the sea states. In future works, ERA20 and ERA5 datasets could be treated as realizations of long-term joint distributions of significant wave heights and peak periods. Factoring in the long-term probability of the sea states would also impact the conclusions here [38].

(a) H_s (b) T_p

Fig. 6. Significant wave height (a) and peak wave period (b) trend from 1900 until 2010 at the study gridpoint. Both present a significant increment at 95% confidence level between 15 and 20% per century. The slope line is computed using Theil-Sen method [18] and the shaded area around it shows the CI (95%).

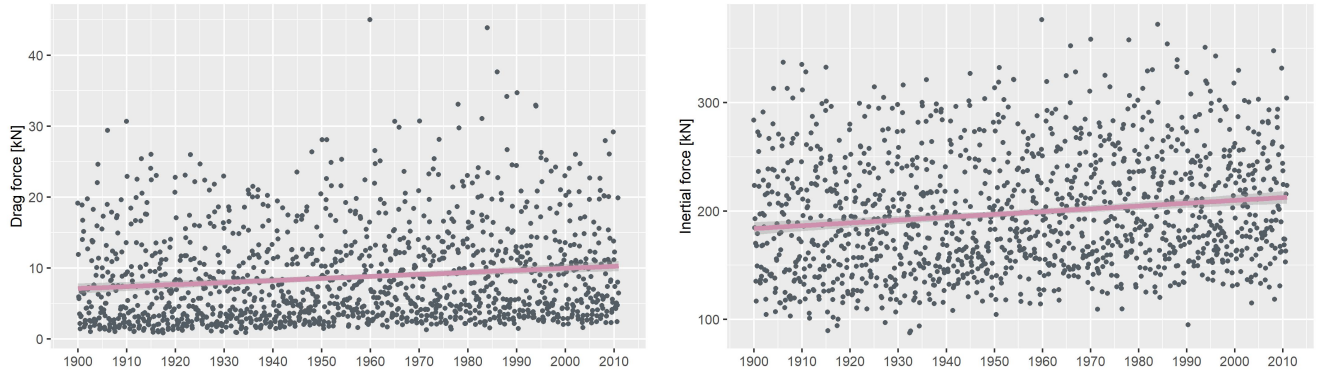

(a) F_D (b) F_I

Fig. 7. Trend of drag and inertial force generated by waves against a monopile structure of 6 meters diameter at a depth of 20 meters in the Bay of Biscay, over a period of 111 years (1900-2010). The slope line is computed using Theil-Sen method [18] and the shaded area around it shows the CI (95%).

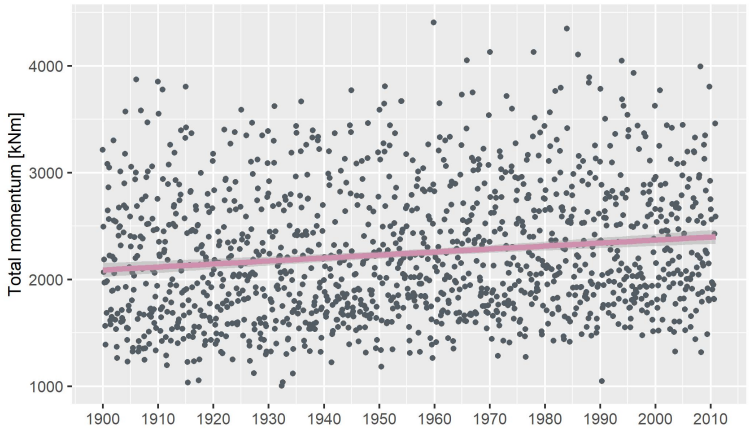

Fig. 8. Trend of total moment at seabed, sum of inertial and drag moment contribution along the monopile submerged at 20 m. The slope line is computed using Theil-Sen method [18] and the shaded area around it shows the CI (95%).

ACKNOWLEDGEMENT

This publication is part of a Grant from Science Foundation Ireland under Grant number 18/CRT/6049. This paper is also part of project PID2020-116153RB-I00 funded by MCIN/AEI/10.13039/501100011033 and has also received funding from the University of the Basque Country (UPV/EHU project GIU20/08).

REFERENCES

[1] *Historia Erdi Aora, Ekonomia, Arrantza*. [Online]. Available: https://www.euskadi.eus/web01-a2lurent/eu/contenidos/articulo/c0504/eu_d0504006/0504006.html
[2] R. U. Ayo, "Anglo-spanish trade through the Port of Bilbao during the second half of the eighteenth century: some preliminary findings," *International Journal of Maritime History*, vol. 4, no. 2, pp. 193–217, 1992.
[3] "Tecnalia," [Last accessed 19/05/2023]. [Online]. Available: https://www.tecnalia.com/

[4] "Renewable Energy in the Marine enviroment," [Last accessed 19/05/2023]. [Online]. Available: https://www.master-rem.eu/

[5] "Ocean Energy Europe 2022," [Last accessed 19/05/2023]. [Online]. Available: https://icoeoee2022donostia.org/

[6] "Ewtec 2023," [Last accessed 19/05/2023]. [Online]. Available: https://ewtec.org/ewtec-2023/

[7] "World Maritime Week 2023," [Last accessed 19/05/2023]. [Online]. Available: https://wmw.bilbaoexhibitioncentre.com/en/

[8] "Biscay Marine Energy Platform," [Last accessed 22/05/2023]. [Online]. Available: https://www.bimep.com/en/bimep-area/services/

[9] "Plan de Ordenacion del Espacio Maritimo," [Last accessed 22/05/2023]. [Online]. Available: https://www.miteco.gob.es/es/costas/temas/proteccion-medio-marino/ordenacion-del-espacio-maritimo/

[10] L. M. Bricheno and J. Wolf, "Future wave conditions of europe, in response to high-end climate change scenarios," *Journal of Geophysical Research: Oceans*, vol. 123, no. 12, pp. 8762–8791, 2018.

[11] S. Aasen, A. M. Page, K. Skjolden Skau, and T. A. Nygaard, "Effect of foundation modelling on the fatigue lifetime of a monopile-based offshore wind turbine," *Wind Energy Science*, vol. 2, no. 2, pp. 361–376, 2017.

[12] ECMWF, "Copernicus data store," https://cds.climate.copernicus.eu/cdsapp, 2023, accessed: 23-May-2023.

[13] H. Hersbach *et al.*, "The era5 global reanalysis," *Quarterly Journal of the Royal Meteorological Society*, vol. 146, no. 730, pp. 1999–2049, 2020.

[14] D. I. Berry and E. C. Kent, "A new air–sea interaction gridded dataset from icoads with uncertainty estimates," *Bulletin of the American Meteorological Society*, vol. 90, no. 5, pp. 645–656, 2009.

[15] P. Poli *et al.*, "ERA-20C: An atmospheric reanalysis of the twentieth century," *Journal of Climate*, vol. 29, no. 11, pp. 4083–4097, 2016.

[16] L. Mentaschi, M. I. Vousdoukas, E. Voukouvalas, A. Dosio, and L. Feyen, "Global changes of extreme coastal wave energy fluxes triggered by intensified teleconnection patterns," *Geophys. Res. Lett.*, vol. 44, pp. 2416–2426, 2017.

[17] J. Jonkman and W. Musial, "Offshore code comparison collaboration (oc3) for iea wind task 23 offshore wind technology and deployment," National Renewable Energy Lab.(NREL), Golden, CO (United States), Tech. Rep., 2010.

[18] H. Theil, "A rank-invariant method of linear and polynomial regression analysis, 3; confidence regions for the parameters of polynomial regression equations," *Stichting Mathematisch Centrum. Statistische Afdeling*, pp. 1–16, 1950.

[19] C. Teutschbein and J. Seibert, "Bias correction of regional climate model simulations for hydrological climate-change impact studies: Review and evaluation of different methods," *Journal of Hydrology*, vol. 456, pp. 12–29, 2012.

[20] S. Watanabe, S. Kanae, S. Seto, P. J.-F. Yeh, Y. Hirabayashi, and T. Oki, "Intercomparison of bias-correction methods for monthly temperature and precipitation simulated by multiple climate models," *Journal of Geophysical Research: Atmospheres*, vol. 117, no. D23, 2012.

[21] P. E. Bett, H. E. Thornton, and R. T. Clark, "Using the Twentieth Century Reanalysis to assess climate variability for the European wind industry," *Theoretical and Applied Climatology*, 2015.

[22] D. Li, J. Feng, Z. Xu, B. Yin, H. Shi, and J. Qi, "Statistical bias correction for simulated wind speeds over CORDEX-East asia," *Earth and Space Science*, vol. 6, no. 2, pp. 200–211, 2019.

[23] K. Whan, J. Zscheischler, A. I. Jordan, and J. F. Ziegel, "Novel multivariate quantile mapping methods for ensemble post-processing of medium-range forecasts," *Weather and Climate Extremes*, vol. 32, p. 100310, 2021.

[24] S. Carreno-Madinabeitia, G. Ibarra-Berastegi, J. Sáenz, and A. Ulazia, "Long-term changes in offshore wind power density and wind turbine capacity factor in the Iberian Peninsula (1900–2010)," *Energy*, vol. 226, p. 120364, 2021.

[25] A. Ulazia, M. Penalba, G. Ibarra-Berastegui, J. Ringwood, and J. Saénz, "Wave energy trends over the bay of biscay and the consequences for wave energy converters," *Energy*, vol. 141, pp. 624–634, 2017.

[26] A. Ulazia, M. Penalba, A. Rabanal, G. Ibarra-Berastegi, J. Ringwood, and J. Sáenz, "Historical evolution of the wave resource and energy production off the Chilean coast over the 20th century," *Energies*, vol. 11, no. 9, p. 2289, 2018.

[27] M. Penalba, A. Ulazia, G. Ibarra-Berastegui, J. Ringwood, and J. Sáenz, "Wave energy resource variation off the west coast of ireland and its impact on realistic wave energy converters' power absorption," *Applied energy*, vol. 224, pp. 205–219, 2018.

[28] A. Ulazia, M. Penalba, G. Ibarra-Berastegui, J. Ringwood, and J. Sáenz, "Reduction of the capture width of wave energy converters due to long-term seasonal wave energy trends," *Renewable and Sustainable Energy Reviews*, vol. 113, p. 109267, 2019.

[29] M. Penalba, A. Ulazia, J. Saénz, and J. V. Ringwood, "Impact of long-term resource variations on wave energy farms: The icelandic case," *Energy*, vol. 192, p. 116609, 2020.

[30] B. Le Méhauté, *An introduction to hydrodynamics and water waves*. Springer Science & Business Media, 2013.

[31] V. Sundar, *Ocean wave mechanics: Applications in marine structures*. John Wiley & Sons, 2017.

[32] B. Barahona, J. M. Jonkman, R. Damiani, A. Robertson, and G. Hayman, "Verification of the new FAST v8 capabilities for the modeling of fixed-bottom offshore wind turbines," in *33rd Wind Energy Symposium*, 2015, p. 1205.

[33] D. Veldkamp, "Chances in wind energy–a probabilistic approach to wind turbine fatigue design [Ph.D thesis]," *Delft University of Technology*, 2006.

[34] R. Burrows, R. Tickell, D. Hames, and G. Najafian, "Morison wave force coefficients for application to random seas," *Applied Ocean Research*, vol. 19, no. 3-4, pp. 183–199, 1997.

[35] J. S. Chung, "Morison equation in practice and hydrodynamic validity," *International Journal of Offshore and Polar Engineering*, vol. 28, no. 01, pp. 11–18, 2018.

[36] J. Jonkman, "Fast: An open-source platform for wind turbine multi-physics engineering modeling," *NAWEA 2017 Symposium*, 2017. [Online]. Available: https://www.aere.iastate.edu/nawea2017/files/2017/09/FASTWorkshop_NAWEA_Jonkman.pdf

[37] I. R. Young, "Regular, irregular waves and the wave spectrum," *Encyclopedia of Maritime and Offshore Engineering*, pp. 1–10, 2017.

[38] J. T. Sørensen, H. Hansen, X. Mandviwalla, F. Pierella, and H. Bredmose, "Direct and fast probabilistic assessment of long term monopile load distribution from combined metocean data and fully nonlinear wave kinematics," in *Journal of Physics: Conference Series*, vol. 2018, no. 1. IOP Publishing, 2021, p. 012037.